The microstructure and hardness of Ni-Co-Al-Ti-Cr quinary alloys

K. A. Christofidou[1], N. G. Jones[1], E. J. Pickering[1,2], R. Flacau[3] M. C. Hardy[4] and H. J. Stone[1]

[1]Department of Materials Science and Metallurgy, University of Cambridge, 27 Charles Babbage Road, Cambridge, CB3 0FS, UK

[2]School of Materials, The University of Manchester, Manchester, M13 9PL, UK

[3]Canadian Neutron Beam Center, Chalk River Laboratories, Chalk River, Ontario, Canada

[4]Rolls-Royce plc, PO Box 31, Derby, DE24 8BJ, UK

Abstract

The effects of Ni:Co and Al:Ti ratios on the room temperature microstructure, hardness and lattice parameter of twenty-seven quinary Ni-Co-Al-Ti-Cr alloys have been evaluated. All of the alloys exhibited a uniform γ-γ′ microstructure. Differential scanning calorimetry (DSC) showed that the liquidus and solidus temperatures of the alloys, increase with greater Al:Ti ratios, decrease with Cr concentration and remained largely unchanged with respect to the Ni:Co ratio. Neutron diffraction measurements of the γ and γ′ lattice parameters revealed that the lattice misfit in all of the alloys was positive and increased with Ti concentration (i.e. lower Al:Ti ratio) regardless of the concentration of Cr, or the ratio of Ni:Co. Importantly, alloys with a Ni:Co ratio of 1:1, were found to have consistently greater lattice misfits than alloys with Ni:Co ratios of either 1:3 or 3:1. The measured lattice misfits were found to be strongly correlated with the Vickers hardness of the alloys, suggesting that lattice misfit plays a key role in the strengthening of γ- γ′ alloys of this type.

1. Introduction

Superalloys based on the Ni-Al-Cr system and comprising up to 12 alloying elements are widely used for components in the hottest sections of gas turbine engines. In civil aviation, regulatory and economic pressures are driving the design of new gas turbine engines towards higher operating temperatures and faster rotation speeds [1-3]. Currently available alloys are already working close to their temperature and strength limits, thereby necessitating the development of new materials capable of withstanding the inimical conditions that will be encountered in the hottest sections of future, more efficient, engines. However, despite significant research to develop alternative materials [4-8], the exceptional balance of properties offered by superalloys with fine scale dispersions of $L1_2$ γ′ precipitates in an A1 γ matrix, continues to make them the preferred solution for high temperature structural applications. Therefore, identifying alloying strategies that can extend the capabilities of A1 – $L1_2$ superalloys continues to be a key research activity in the aerospace industry.

Cobalt is an attractive option for next generation A1 – $L1_2$ superalloys as its metallurgy is remarkably similar to that of nickel, with the added advantage of a higher melting point. Co-based alloys containing $L1_2$ precipitates were identified in the Co – Ti and Co – Ta systems in the 1960s [9,10]. However, as a consequence of the successful development of Ni-based superalloys, and the uncertainty in the global supply of Co at that time, commercial interest in these systems waned. In the 1970s, Viatour *et al.* [11] developed multi-component Co-based alloys reinforced with Co_3Ti precipitates, but these alloys were unable to compete with the balance of properties offered by their Ni-based counterparts. More recently, Sato *et al.* [12] reported the existence of an A1 – $L1_2$ two phase field between a Co solid solution and the $Co_3(Al,W)$ phase in the Co – Al – W ternary system. In the ten years since this discovery, considerable work has been performed to gain an enhanced understanding of the behaviour of these materials and develop commercially viable alloys. This research has included studies of the phase equlibria and the effect of alloying [13-27], evaluation of their deformation behaviour [22,28-41], and assessment of their environmental resistance [42-44]. However, despite exhibiting several beneficial attributes, further development is still required before any of these alloys can compete with existing Ni-based superalloys.

At the same time as the discovery of the Co – $Co_3(Al,W)$ system, separate research efforts investigated the properties of Ni-based superalloys with high Co & Ti concentrations to induce the precipitation of the $L1_2$ - Co_3Ti phase [45,46]. Such modifications were shown to confer benefits to both the strength and microstructural stability of both cast & wrought [47-51] and powder processed [52,53] alloys. In parallel, fundamental studies of the underpinning Ni – Co – Al – Ti system were performed and determined that the A1 – $L1_2$ two-phase field is continuous between Ni – Ni_3Al and Co – Co_3Ti [54,55]. More recently, Oni *et al.* [56] employed a range of advanced characterisation techniques to study the site occupancies and lattice misfit strains in quaternary Ni-Co-Al-Ti alloys, and demonstrated a more complicated partitioning and site occupancy behaviour for Co than initially expected. However, whilst co-additions of

Co & Ti are clearly beneficial to the properties of Ni-based superalloys, the origins of these effects have not yet been conclusively established.

To gain further insight into the physical metallurgy of Ni-based superalloys with elevated Co & Ti concentrations, several compositions from within the Ni – Co – Al – Ti – Cr quinary system have been examined following a super-solvus homogenisation heat treatment. In this condition, all of the alloys were found to have a γ – γ′ microstructure and their transition temperatures, microstructural characteristics, hardness and lattice parameters have been evaluated. From these data, the effects of varying the Ni:Co and Al:Ti ratios at three distinct Cr concentrations were assessed.

2. Experimental

Twenty-seven alloys were selected from the $(Ni,Co)_{90-x}(Al,Ti)_{10}Cr_x$ system, where x = 10, 15 or 20 at.%. At each Cr concentration, the relative ratios of Ni:Co and Al:Ti were independently varied from 3:1, to 1:1 to 1:3. The nominal compositions of the alloys are shown in Table 1. The naming convention of the alloys was chosen to reflect the composition ratios as follows: the first 2 numbers denote the chromium content in the alloy, for example an alloy containing a nominal 15 at. % Cr was named 15##; the subsequent number reflects the ratio of Ni:Co, number '1' was used to denote a Ni:Co ratio of 1:3, '2' denoted a Ni:Co ratio of 1:1 and '3' denoted a Ni:Co ratio of 3:1, similarly, the last letter was used to identify the Al:Ti ratio, with 'a' indicating a ratio of 1:3, 'b' indicating a ratio of 1:1 and 'c' indicating a ratio of 3:1.

The alloys were produced by arc melting elements of ≥ 99.9% purity under an inert atmosphere. Each ingot was inverted and remelted a total of five times to minimise compositional inhomogeneity. Differential scanning calorimetry (DSC) data was acquired from 3 mm diameter, 1 mm thick samples using a SETARAM SETSYS Evolution DSC/TGA instrument. The heat flux was measured on heating between 700˚C and 1450˚C under an inert atmosphere using a heating rate of 10˚C min^{-1}. The solidus temperatures were identified from the DSC thermograms in line with the NIST recommendations [57]. This enabled homogenisation heat treatment temperatures to be identified close to the solidus, whilst avoiding incipient melting. Due to the logistics of heat treating 27 separate ingots, the alloys were grouped and heat treated at three temperatures; 1150, 1200 and 1250˚C, for 48 hours, followed by air cooling. To protect the samples from oxidation during the homogenisation heat treatments, each ingot was encapsulated in an argon backfilled quartz ampoule.

The homogenised bars were also characterised using DSC, with the same protocol as the as-cast samples, to determine the liquidus, solidus and solvus temperatures of the alloys in this condition. In order to compare the measured transition temperatures with those predicted using thermodynamic models, calculations were performed on all 27 compositions using the Thermo-Calc software with both the TCNi5 and TTNi8 thermodynamic databases. No phases were omitted in conducting these calculations.

Microstructural characterisation was performed on samples which had been polished and electrolytically etched using a 10% phosphoric acid solution at ≈3 V. Imaging was conducted using an FEI Helios Dual Beam system and a JEOL FEG6340 scanning electron microscope (SEM), whilst quantitative compositional analysis was performed on a JEOL 5800 SEM equipped with an Oxford instruments energy dispersive X-ray spectroscopy (EDX) system. Bulk compositions were determined from the average of five 500 x 500 µm EDX scans. Transmission electron microscopy (TEM) was performed on alloys 101a, 151a and 201a in the as-homogenised condition, using an FEI Tecnai Osiris operated at 200 kV. Bright-field and high-angle-annular dark field (HAADF) images were acquired in scanning – TEM (STEM) mode. The γ′ particle size was obtained from the TEM images using the ImageJ software package. Room temperature hardness data were collected from polished samples using a Vickers hardness indenter with a 2 kg mass and 30 s dwell. The value reported was the average of eight individual measurements and the error quoted was the standard deviation of these measurements.

Neutron diffraction was used to measure the lattice parameters of the phases present in each alloy. Data was collected on the C2 high-resolution powder diffractometer at the Canadian Neutron Beam Center (CNBC) using monochromatic neutrons with a wavelength of 1.33 Å, as determined from calibration with an Al_2O_3 standard. The BF3 position sensitive detector on C2, which consists of 800-wires spaced 0.1˚ apart, allowed the simultaneous collection of diffraction data over an 80˚ angular range in 2θ. For the purposes of this study, the 2θ range between 37-117˚ was deemed most suitable, as this enabled characterisation of reflections between {111} & {331} from both the A1 and $L1_2$ phases. A data acquisition time of 3 hours was required in order to obtain sufficient statistics to resolve the superlattice reflections. Data analysis was performed with the TOPAS academic software, using the Pawley [58] fitting procedure. An example of fitted data is shown in Figure 1. The lattice misfit of the alloys, and the associated errors, were calculated from the lattice parameters obtained from the fitting procedure using Equation 1, in which δ denoted the percentage lattice misfit and α_γ and $\alpha_{\gamma'}$ corresponded to the lattice parameters of the γ and γ′ phases respectively.

$$\delta = 2 \times \left[\frac{\alpha_{\gamma'} - \alpha_\gamma}{\alpha_{\gamma'} + \alpha_\gamma}\right] \times 100 \qquad \text{Equation 1}$$

3. Results

3.1 DSC results

The DSC thermograms acquired from the homogenised samples were analysed in order to obtain the transformation temperatures. Whilst the NIST guidelines were used when obtaining the liquidus and solidus temperature [57], the precipitate solvus temperatures were determined as the first deviation from the baseline on heating, as this indicated the beginning of precipitate dissolution rather than the maximum rate of dissolution [59].

The transformation temperatures from each alloy are given in Table 1. These data suggested that increasing the Cr concentration decreased the liquidus and solidus temperatures of the alloys, with the effect on the solidus temperature being more pronounced. Conversely, increasing the Al:Ti ratio raised the liquidus and the solidus temperatures of the alloys. However, variations in the Co concentration did not cause significant changes in either of these temperatures.

The data also indicated that the solvus temperature was depressed as the Al:Ti ratio increased and this effect was larger in alloys with higher Co concentrations. Increasing the Co concentration produced a similar effect on the solvus temperature, whilst variations in the Cr concentration did not alter the solvus temperatures appreciably.

3.2 Thermodynamic modeling results

The liquidus, solidus and solvus temperatures calculated using thermodynamic modelling are presented in Table 2. The liquidus and solidus temperatures were predicted by both databases to increase with the Al:Ti ratio and decrease with increasing Cr concentration. Varying the Ni:Co ratio did not appear to influence these transformation temperatures. Both databases also suggested that the γ′ solvus temperature should increase with Cr concentration and decrease with higher Al:Ti ratios. The effect of the Ni:Co ratio on the γ′ solvus was more complicated. Calculations made using the TCNi5 database suggested that the γ′ solvus temperature should increase with the Ni:Co ratio for alloys with Al:Ti ratios equal to 1:1 and 3:1, but not for alloys with Al:Ti ratio equal to 1:3. In contrast, using the TTNi8 database, an increase in the γ′ solvus was predicted with the Ni:Co ratio for the alloys that contained an Al:Ti ratio equal to 1:3. In addition, alloys that had an Al:Ti ratio of 3:1 were predicted to have γ′ solvus temperatures that increased only with Cr concentrations of 15 and 20 at.%. Both databases also suggested that additional intermetallic phases should form; TCNi5 predicted the formation of the η, β and σ phases in some alloys, whereas the TTNi8 database predicted much greater prevalence of the η phase and more limited β phase formation.

3.4 Microstructures

Secondary electron micrographs of all the alloys after homogenisation for 48 hours are shown in Figures 2, 3 and 4. A uniform γ – γ′ microstructure was observed in all alloys, albeit that the size and volume fraction of the γ′ precipitates varied considerably as a function of composition. In most Co-rich alloys, ##1# type, the γ′ precipitates could not be resolved using SEM, and hence, their volume fraction and distribution could not be accurately determined from the micrographs. The morphology of the γ′ precipitates did not appear to be significantly affected by the composition of the alloys. In contrast, the correlation between precipitate size and elemental concentration was more easily discerned. From the images acquired, larger γ′ precipitates were observed with higher Ni:Co ratios, lower Al:Ti ratios or increased Cr concentrations.

3.5 Hardness

The variation of alloy hardness as a function Ti & Al concentration for the three levels of Cr are shown in Figure 5 a-c. The hardness values showed a monotonic increase with Ti concentration, corresponding to lower Al:Ti ratios, with the exception of alloy 202b, which showed an anomalously low hardness. In addition, the Co-based alloys (##1#) displayed consistently lower hardness values than their Ni- and Ni-Co-based counterparts, which showed similar hardness values, with the exception of alloy 101a that exhibited a unusually high hardness.

3.6 Lattice parameters and lattice misfit

The lattice parameters of the γ and γ′ phases, determined from Pawley analysis of the neutron diffraction data, are presented in Figure 5 d-f. In all alloys, the lattice parameter of the γ′ phase was consistently larger than that of the γ phase. In line with the variation in hardness, elevated concentrations of Ti, corresponding to low Al:Ti ratios, gave rise to increased lattice parameters of both the γ and γ′ phases, with the effect being greater in the γ′ phase. Similarly, increasing the Cr concentration caused an expansion in the lattice parameters of both phases, but in this case, the effect was more pronounced in the γ phase. Small increases in the lattice parameter of the γ phase were also observed with increasing Co concentration, corresponding to lower Ni:Co ratios, although the γ′ lattice parameter remained largely unchanged. As before, alloy 202b was the exception to all of the aforementioned trends.

The lattice misfit calculated from the measured lattice parameters as a function of Ti & Al concentration is shown in Figure 5 g-i. All of the alloys considered here had positive lattice misfits that increased with the concentration of Ti (decreasing Al:Ti ratio). The lattice misfit was also observed to decrease with elevated Cr concentrations in the Ni and Ni-Co alloys, but not in alloys rich in Co. In addition, the alloys based on an equiatomic Ni-Co matrix, ##2# type alloys, showed consistently larger lattice misfit values than their Ni- or Co-rich counterparts. Again, alloy 202b was the exception and did not conform with either of these trends.

4. Discussion

The liquidus, solidus and solvus temperatures obtained from the DSC data were found to vary with alloy composition. The changes in these temperatures with increasing Cr concentration were consistent with results previously reported in the literature [60-62], as was the decrease in the γ′ solvus with increasing Co concentration [63,64]. However, not all of the trends were consistent with previous studies. Zhi'an *et al.* [65] presented data that showed that Co raised the solidus temperature when substituted for Ni, whereas Stephens *et al.* [64] reported the opposite trend. In this study, Co was found to have a negligible effect on the solidus temperature of the alloys examined.

The key transition temperatures predicted with the TCNi5 and TTNi8 databases, Table 2, showed significant differences. The liquidus and solidus temperatures calculated using the TTNi8 database were consistently higher than the equivalent values obtained using the TCNi5 database, with the exception of alloy 203c. Despite the difference in absolute values, the trends predicted for the liquidus and solidus temperatures as a function of alloy composition were reasonably consistent between the two databases. The most significant discrepancy between the two databases was the additional intermetallic phases predicted to form in the alloys and their associated solvus temperatures.

As a result of the increasing popularity of thermodynamic predictions in the design of multicomponent alloys, it is vital that the limitations of current databases are understood by comparing the computed data to experimental results. In Figure 6, the experimentally obtained liquidus and solidus temperatures are plotted as a function of the equivalent calculated temperatures and, in each case, the line across the graphs represents the line of absolute agreement between the calculations and the DSC results.

The liquidus temperatures predicted using both databases were in reasonable agreement with the liquidus temperatures measured using DSC, with a maximum discrepancy of about 25˚C, although the scatter in the data calculated using the TCNi5 database was much greater. Inferior agreement was obtained between the experimental and predicted solidus temperatures. The solidus temperatures calculated with the TTNi8 database were consistently higher than the corresponding values obtained using DSC, but both datasets showed similar trends. In contrast, the predictions made with the TCNi5 database were in closer agreement with the experimental results, although differences up to 150˚C were observed. Whilst the majority of alloy compositions tested contained Co contents that were much greater than conventional Ni-based superalloys and, therefore, lie outside of the databases' assessed composition space where predictions are expected to be reliable, the inconsistencies extended to compositions that were considered to be well within the assessed space.

Critically, all of the experimental data were collected from samples that had only undergone a homogenisation heat treatment, with no additional ageing heat treatment. As such, thermodynamic equilibrium of the precipitating phases was not established in the alloys, hence, no comparison can be directly made between the predicted solvus temperatures and those determined experimentally.

The solvus temperatures measured using DSC can be used to account for the relative γ′ precipitate sizes observed in Figures 2, 3 and 4. Since the material was not subjected to an ageing heat treatment to modify the precipitate distribution, the formation and growth of the γ′ precipitates will have been confined to the cooling period following the homogenisation heat treatment. As a consequence, the precipitate size may be expected to be dependent on the γ′ solvus temperature. This is consistent with the experimental observations, with alloys having lower γ′ solvus temperatures exhibiting finer precipitate sizes. Conversely, those alloys with higher Ni and/or Ti contents, which exhibited higher solvus temperatures, led to larger γ′ precipitates [66]. Importantly, no strong correlation between the solution heat treatment temperature and the resulting γ′ precipitate size was observed.

The lattice parameters of the γ and γ′ phases were both observed to increase as a function of Ti and Cr content. Notably, the Ti concentration had a greater influence on the γ′ lattice parameter whereas the Cr concentration had a more pronounced effect on the lattice parameter of the γ phase. These observations allude to preferential partitioning of Ti towards the γ′ phase and Cr towards the γ phase, consistent with previous reports [67-69] As a consequence, the differential changes in the lattice parameters of the individual phases arising as a result of these additions were reflected in the lattice misfits obtained. The greater increase in the γ′ lattice parameter associated with Ti additions led to a larger lattice misfit, whilst Cr additions had the opposite effect, leading to a smaller lattice misfit.

As detailed testing of the mechanical properties of the alloys was impractical given the small volumes of material available for the twenty-seven alloys investigated, hardness measurements were taken as a proxy for their strength to allow a preliminary assessment of the effect of alloying. With the exception of alloy 202b, the hardness of the alloys studied was observed to increase with the Ti concentration. Ti is known to be a potent γ′ strengthener, substituting

onto the Al sublattice of the $L1_2$ structure, increasing both the anti-phase boundary (APB) energy and the lattice misfit [70-73].

A plot of hardness as a function of lattice misfit for all alloys examined in this study is shown in Figure 7. A strong correlation between these two quantities is apparent from the figure, but as both lattice misfit and APB energy are related to Ti content, this alone cannot distinguish their relative contributions. The respective potencies of these strengthening mechanisms can be elucidated from the data presented in Figure 5. For alloys with constant Al:Ti and Ni:Co ratios, elevated Cr concentrations would be expected to harden the alloy by additional solid solution strengthening of the γ matrix, increasing the γ′ volume fraction by reducing the solubility of both Al and Ti in the matrix and, provided this leads to an increase in the concentration of Ti in the γ′ precipitates, increasing the APB energy. However, as noted earlier, Cr additions also increased the lattice parameter of the γ phase, thereby decreasing the lattice misfit. Therefore, by considering the change in hardness of alloys with constant Al:Ti and Ni:Co ratios and varying Cr concentrations, it is possible to gain an insight into the relative potency of lattice misfit on alloy strength.

The hardnesses measured on the alloys containing 7.5 at. % Ti and a Ni:Co ratio of 1:3, varied from 457 Hv for the alloy with 10 at.% Cr, to 395 Hv for the alloy with 15 at.% Cr and 369 Hv for the alloy with 20 at.% Cr. These hardness values indicate that, despite Cr promoting several strengthening mechanisms, the reduction in lattice misfit that it produces has a greater effect upon the overall strength of the alloy. Similar decreases in hardness with increasing Cr concentration can be observed in the majority of the other alloy series, thereby suggesting that lattice misfit is indeed a potent strengthening mechanism in the alloys examined. Furthermore, in those alloy series that do not show this trend as clearly, a strong correlation between the measured lattice misfit and the hardness still exists. For example, the alloys containing 5 at.% Ti and a Ni:Co ratio of 1:3 show little variation in hardness but also display no significant difference in lattice misfit. Similarly, the anomalously low hardness of alloy 202b is reflected in an anomalously low lattice misfit.

The preceding argument has not considered the effect of precipitate size on the measured hardnesses. Recent work on Ni – Cr – Al – Nb alloys showed that decreasing the size of the γ′ precipitates resulted in appreciable strengthening [74], in line with classical models of precipitation hardening [70]. The extent to which precipitate size contributed to the hardness of the alloys in this study can again be understood by comparing alloys with 7.5 at.% Ti and a Ni:Co ratio of 1:3. However, as the size of the precipitates in these alloys could not be reliably determined from the SEM micrographs presented in Figures 2, 3 and 4, higher resolution TEM was performed. The precipitate sizes determined through analysis of the TEM images obtained are provided in Table 3, along with the corresponding lattice misfit and hardness values. Alloys 101a and 201a had similar γ′ sizes of ~ 46 nm, whilst the precipitates in 151a were slightly larger at ~ 59 nm. These precipitate sizes are not obviously correlated with the measured hardness values. This is particularly evident when considering alloys 101a and 201a, which have nearly identical precipitate sizes yet exhibit a ~ 90 Hv difference in hardness. In contrast, the measured hardness values can be directly correlated to the lattice misfit, with greater lattice misfit leading to a concomitant increase in hardness. Therefore, whilst previous work has clearly shown that precipitate size is an important contributor to alloy strength, the ability to rationalise all of the significant hardness variations in the present work through lattice misfit makes a compelling argument that this mechanism also plays a key role in strengthening A1 – $L1_2$ superalloys.

Several studies have sought to quantify the effect of lattice misfit and coherency strengthening on the mechanical properties of superalloys [72,75-79]. Gerold and Haberkorn [75] used rigorous mathematical analyses combining linear elasticity theory with statistical approximations to formulate the interactions of the precipitate stress field with a dislocation, assuming a spherical stress field, a straight dislocation line and an elastically isotropic matrix. The results obtained in their study, indicated that for an edge dislocation, the change in the CRSS should be proportional to the absolute value of $\delta^{3/2}$. However, this result was only applicable to alloys in which deformation occurs through dislocation cutting of the precipitates, therefore, underaged alloys. Ardell [78] in his 1985 review of precipitation hardening, offered a thorough explanation of the limitations of the theoretical mathematical approaches used to that date, and suggested that these arise primarily from the statistical averaging operations required and due to the assumptions associated with the deformation mechanism. In contrast to the theoretical approaches used by most researchers, Grose and Ansell [77], followed an empirical, experimental approach, in which a set of alloy compositions were designed in order to isolate and examine various aspects of strengthening behaviour. The results obtained indicated that for alloys in which the lattice misfit was high, the flow stress (normalised against volume fraction) displayed a very strong near-linear dependence on the lattice misfit. A much weaker dependence of the normalised flow stress on the lattice misfit was found in alloys with low lattice misfits, in which the behaviour observed was believed to be dominated by the APB and stacking fault energies of the material.

As discussed earlier, in the current study a near-linear correlation was obtained between the alloy hardness and the constrained lattice misfit, as shown in Figure 7. Whilst the collective results exhibited significant scatter, clearer trends were observed when the data was further subdivided into three categories depending on the predominant element in the alloy i.e. Ni-based, Co-based and NiCo-based alloys. A line was fitted through the data points from each category and these suggested that the hardness of Ni-based alloys and those with equiatomic concentrations of Ni & Co (NiCo-based alloys) showed similar dependence on lattice misfit. In contrast, the hardnesses of the Co-based alloys showed a greater dependence on the lattice misfit, with a change of 0.1% in the lattice misfit increasing the hardness by ~ 70 Hv. However, three compositions were found to only loosely depend on the lattice misfit, and displayed hardness values of ~ 250 Hv. Whilst these results appear to be consistent with the findings of Grose and Ansell [77] who suggested that low lattice misfit alloys are less dominated by coherency strengthening, removing these three data

points did not produce a considerable change in the variation of alloy hardness with lattice misfit (0.1% change in the misfit was translated to a ~ 60Hv change in the hardness). This suggests that Co-based alloys may indeed be more strongly dependent upon lattice misfit than their Ni-based or NiCo-based counterparts.

5. Conclusions

A series of twenty-seven alloys from the Ni – Co – Al – Ti – Cr system were investigated using DSC, SEM, neutron diffraction and hardness measurements. All of the alloys examined exhibited a uniform γ – γ′ microstructure, with positive lattice misfits. The liquidus and solidus temperatures of the alloys were found to increase with the Al:Ti ratio, decrease with the Cr concentration, and remain largely unchanged with the variation of Ni:Co ratio. In contrast, the precipitate solvus temperatures increased with the Ni:Co ratio, but decreased with an increasing Al:Ti ratio and no discernible effects were obtained with the variation in the concentration of Cr. Thermodynamic predictions of the transition temperatures from all compositions were compared against the temperatures obtained using DSC and revealed large discrepancies, suggesting that thermodynamic modelling should be used with caution.

The lattice parameters of the γ and γ′ phases were measured using neutron diffraction and were found to increase with the concentration of Ti and Cr, whilst no significant variation was observed with changes in the Ni:Co ratio. More importantly, the effects of these elements on the lattice parameters were reflected in the corresponding lattice misfits, which increased with higher concentrations of Ti and decreased with elevated Cr contents.

The hardness values of all of the alloys were found to be strongly correlated with the measured lattice misfits. Detailed analysis of three alloys confirmed this observation, although the precise functional dependence could not be determined due to the effects of other strengthening mechanisms, including precipitate size. However, the strong correlation observed clearly shows that lattice misfit plays a key role in strengthening A1 – $L1_2$ superalloys.

Acknowledgements

The authors would like to thank Mr. K. A. Roberts and Dr. H. T. Pang for experimental assistance, and Dr. P. M. Mignanelli for useful discussions. This work was supported by the Rolls-Royce / EPSRC Strategic Partnership under EP/H022309/1, EP/H500375/1 and EP/M005607/1. The Canadian Neutron Beam Centre is also acknowledged for the provision of beam time under CNBC-1007.

Bibliography

[1] European Aeronautics: A Vision for 2020, European Commission, 2001.
[2] Flightpath 2050 Europe's vision for aviation, European Commission, 2011. doi:10.2777/50266.
[3] Advisory Council for Aeronautics Research in Europe, ACARE Handover-Document, 2011.
[4] A. Bhowmik, H.J. Stone, Microstructure and Mechanical Properties of Two-Phase Cr-Cr2Ta Alloys, Metallurgical and Materials Transactions A. 43 (2012) 3283–3292. doi:10.1007/s11661-012-1140-6.
[5] M.G. Mendiratta, D.M. Dimiduk, Strength and toughness of a Nb/Nb_5Si_3 composite, Metallurgical and Materials Transactions A. 24 (1993) 501–504. doi:10.1007/BF02657338.
[6] J. Geng, P. Tsakiropoulos, G. Shao, The effects of Ti and Mo additions on the microstructure of Nb-silicide based in situ composites, Intermetallics. 14 (2006) 227–235. doi:10.1016/j.intermet.2005.04.021.
[7] Y.-W. Kim, Intermetallic alloys based on gamma titanium aluminide, Jom. 41 (1989) 24–30. doi:10.1007/BF03220267.
[8] B.A. Pint, Critical Assessment 4: Challenges in developing high temperature materials, Materials Science and Technology. 30 (2014) 1387–1391. doi:10.1179/1743284714Y.0000000580.
[9] H. Bibring, J. Manenc, Structure des phases dans le système Co-Ti, Academie Des Sciences. (1959) 1508–1510.
[10] M. Korchynsky, R.W. Fountain, Precipitation phenomena in Cobalt-Tantalum alloys, Transactions of the Metallurgical Society of AIME. 215 (1959) 1033–1043.
[11] P. Viatour, J.M. Drapier, D. Coutsouradis, Stability of the γ′-Co_3Ti compound in simple and complex cobalt alloys, Cobalt. 3 (1973) 67–74.
[12] J. Sato, Cobalt-Base High-Temperature Alloys, Science. 312 (2006) 90–91. doi:10.1126/science.1121738.
[13] E.A. Lass, M.E. Williams, C.E. Campbell, K.-W. Moon, U.R. Kattner, γ′ Phase Stability and Phase Equilibrium in Ternary Co-Al-W at 900 °C, Journal of Phase Equilibria and Diffusion. 35 (2014) 711–723. doi:10.1007/s11669-014-0346-2.
[14] P.J. Bocchini, E.A. Lass, K.-W. Moon, M.E. Williams, C.E. Campbell, U.R. Kattner, et al., Atom-probe tomographic study of γ/γ′ interfaces and compositions in an aged Co–Al–W superalloy, Scripta Materialia. 68 (2013) 563–566. doi:10.1016/j.scriptamat.2012.11.035.
[15] A. Mottura, A. Janotti, T.M. Pollock, Alloying Effects in the γ′ Phase of Co- Based Superalloys, John Wiley & Sons, Inc, Hoboken, NJ, USA, 2012. doi:10.1002/9781118516430.ch76.

[16] H.-Y. Yan, J. Coakley, V.A. Vorontsov, N.G. Jones, H.J. Stone, D. Dye, Alloying and the micromechanics of Co–Al–W–X quaternary alloys, Materials Science & Engineering A. 613 (2014) 201–208. doi:10.1016/j.msea.2014.05.044.
[17] H.-Y. Yan, V.A. Vorontsov, J. Coakley, N.G. Jones, H.J. Stone, D. Dye, Quaternary Alloying Effects and the Prospects for a New Generation of Co- Base Superalloys, John Wiley & Sons, Inc, Hoboken, NJ, USA, 2012. doi:10.1002/9781118516430.ch78.
[18] S. Meher, H.Y. Yan, S. Nag, D. Dye, R. Banerjee, Solute partitioning and site preference in γ/γ′ cobalt-base alloys, Scripta Materialia. 67 (2012) 850–853. doi:10.1016/j.scriptamat.2012.08.006.
[19] Y. Liu, M. Tang, Y. Zhang, H. Peng, J. Wang, X. Su, Phase equilibria of the AlCoW system at 600 °C, Journal of Alloys and Compounds. 678 (2016) 193–200. doi:10.1016/j.jallcom.2016.03.264.
[20] C.H. Zenk, S. Neumeier, N.M. Engl, S.G. Fries, O. Dolotko, M. Weiser, et al., Intermediate Co/Ni-base model superalloys — Thermophysical properties, creep and oxidation, Scripta Materialia. 112 (2016) 83–86. doi:10.1016/j.scriptamat.2015.09.018.
[21] W. Xu, Y. Wang, C. Wang, X. Liu, Z.-K. Liu, Alloying effects of Ta on the mechanical properties of γ' Co3(Al, W): A first-principles study, Scripta Materialia. 100 (2015) 5–8. doi:10.1016/j.scriptamat.2014.11.029.
[22] F. Pyczak, A. Bauer, M. Göken, U. Lorenz, S. Neumeier, M. Oehring, et al., The effect of tungsten content on the properties of L12-hardened Co–Al–W alloys, Journal of Alloys and Compounds. 632 (2015) 110–115. doi:10.1016/j.jallcom.2015.01.031.
[23] I. Povstugar, P.-P. Choi, S. Neumeier, A. Bauer, C.H. Zenk, M. Göken, et al., Elemental partitioning and mechanical properties of Ti- and Ta-containing Co–Al–W-base superalloys studied by atom probe tomography and nanoindentation, Acta Materialia. 78 (2014) 78–85. doi:10.1016/j.actamat.2014.06.020.
[24] S. Neumeier, H.U. Rehman, J. Neuner, C.H. Zenk, S. Michel, S. Schuwalow, et al., Diffusion of solutes in fcc Cobalt investigated by diffusion couples and first principles kinetic Monte Carlo, Acta Materialia. 106 (2016) 304–312. doi:10.1016/j.actamat.2016.01.028.
[25] S. Neumeier, L.P. Freund, M. Göken, Novel wrought γ/γ′ cobalt base superalloys with high strength and improved oxidation resistance, Scripta Materialia. 109 (2015) 104–107. doi:10.1016/j.scriptamat.2015.07.030.
[26] J. Koßmann, C.H. Zenk, I. Lopez-Galilea, S. Neumeier, A. Kostka, S. Huth, et al., Microsegregation and precipitates of an as-cast Co-based superalloy—microstructural characterization and phase stability modelling, Journal of Materials Science. (2015) 1–10. doi:10.1007/s10853-015-9177-8.
[27] J. Koßmann, T. Hammerschmidt, S. Maisel, S. Müller, R. Drautz, Solubility and ordering of Ti, Ta, Mo and W on the Al sublattice in L12-Co3Al, Intermetallics. 64 (2015) 44–50. doi:10.1016/j.intermet.2015.04.009.
[28] A. Bauer, S. Neumeier, F. Pyczak, M. Göken, Creep Strength and Microstructure of Polycrystalline γ′ – Strengthened Cobalt- Base Superalloys, John Wiley & Sons, Inc, Hoboken, NJ, USA, 2012. doi:10.1002/9781118516430.ch77.
[29] A. Bauer, S. Neumeier, F. Pyczak, M. Göken, Microstructure and creep strength of different γ/γ′-strengthened Co-base superalloy variants, Scripta Materialia. 63 (2010) 1197–1200. doi:10.1016/j.scriptamat.2010.08.036.
[30] Y.M. Eggeler, M.S. Titus, A. Suzuki, T.M. Pollock, Creep deformation-induced antiphase boundaries in L12-containing single-crystal cobalt-base superalloys, Acta Materialia. 77 (2014) 352–359. doi:10.1016/j.actamat.2014.04.037.
[31] M.S. Titus, Y.M. Eggeler, A. Suzuki, T.M. Pollock, Creep-induced planar defects in L12-containing Co- and CoNi-base single-crystal superalloys, Acta Materialia. 82 (2015) 530–539. doi:10.1016/j.actamat.2014.08.033.
[32] J. Zhu, M.S. Titus, T.M. Pollock, Experimental Investigation and Thermodynamic Modeling of the Co-Rich Region in the Co-Al-Ni-W Quaternary System, Journal of Phase Equilibria and Diffusion. 35 (2014) 595–611. doi:10.1007/s11669-014-0327-5.
[33] A. Suzuki, High-temperature strength and deformation of γ/γ′ two-phase Co–Al–W-base alloys, Acta Materialia. 56 (2008) 1288–1297. doi:10.1016/j.actamat.2007.11.014.
[34] A. Suzuki, G.C. DeNolf, T.M. Pollock, Flow stress anomalies in γ/γ′ two-phase Co–Al–W-base alloys, Scripta Materialia. 56 (2007) 385–388. doi:10.1016/j.scriptamat.2006.10.039.
[35] Y.M. Eggeler, J. Müller, M.S. Titus, A. Suzuki, T.M. Pollock, E. Spiecker, Planar defect formation in the γ′ phase during high temperature creep in single crystal CoNi-base superalloys, Acta Materialia. (2016) 1–15. doi:10.1016/j.actamat.2016.03.077.
[36] Z.M.T. Chen, N.L. Okamoto, M. Demura, H. Inui, Micropillar compression deformation of single crystals of Co3(Al,W) with the L12 structure, Scripta Materialia. 121 (2016) 28–31. doi:10.1016/j.scriptamat.2016.04.029.
[37] S. Meher, G.B. Viswanathan, S. Nag, H.L. Fraser, R. Banerjee, Determination of the gamma prime/gamma interface width in a Co–Al–W alloy via coupled aberration-corrected scanning transmission electron microscopy and atom probe tomography, Scripta Materialia. 121 (2016) 23–27. doi:10.1016/j.scriptamat.2016.04.037.
[38] C.H. Zenk, A. Bauer, P. Goik, S. Neumeier, H.J. Stone, M. Göken, Microstructure, Lattice Misfit, and High-Temperature Strength of γ′-Strengthened Co-Al-W-Ge Model Superalloys, Metallurgical and Materials Transactions A. 47 (2016) 2141–2149. doi:10.1007/s11661-016-3408-8.
[39] C.H. Zenk, S. Neumeier, H.J. Stone, M. Göken, Mechanical properties and lattice misfit of γ/γ′ strengthened Co-base superalloys in the Co–W–Al–Ti quaternary system, Intermetallics. 55 (2014) 28–39. doi:10.1016/j.intermet.2014.07.006.

[40] F. Pyczak, A. Bauer, M. Göken, S. Neumeier, U. Lorenz, M. Oehring, et al., Plastic deformation mechanisms in a crept L12 hardened Co-base superalloy, Materials Science & Engineering A. 571 (2013) 13–18. doi:10.1016/j.msea.2013.02.007.
[41] F. Pyczak, B. Devrient, F.C. Neuner, H. Mughrabi, The influence of different alloying elements on the development of the γ/γ′ microstructure of nickel-base superalloys during high-temperature annealing and deformation, Acta Materialia. 53 (2005) 3879–3891. doi:10.1016/j.actamat.2005.04.041.
[42] L. Klein, A. Bauer, S. Neumeier, M. Göken, S. Virtanen, High temperature oxidation of γ/γ′-strengthened Co-base superalloys, Corrosion Science. 53 (2011) 2027–2034. doi:10.1016/j.corsci.2011.02.033.
[43] L. Klein, A. Zendegani, M. Palumbo, S.G. Fries, S. Virtanen, First approach for thermodynamic modelling of the high temperature oxidation behaviour of ternary γ′-strengthened Co–Al–W superalloys, Corrosion Science. 89 (2014) 1–5. doi:10.1016/j.corsci.2014.08.016.
[44] H.Y. Yan, V.A. Vorontsov, D. Dye, Effect of alloying on the oxidation behaviour of Co–Al–W superalloys, Corrosion Science. 83 (2014) 382–395. doi:10.1016/j.corsci.2014.03.002.
[45] C. Cui, D. Ping, Y. Gu, H. Harada, A New Co-Base Superalloy Strengthened by γ′ Phase, Materials Transactions. 47 (2006) 2099–2102. doi:10.2320/matertrans.47.2099.
[46] D.H. Ping, C.Y. Cui, Y.F. Gu, H. Harada, Microstructure of a newly developed γ′ strengthened Co-base superalloy, Ultramicroscopy. 107 (2007) 791–795. doi:10.1016/j.ultramic.2007.02.010.
[47] Y. Gu, H. Harada, C. Cui, D. Ping, A. Sato, J. Fujioka, New Ni–Co-base disk superalloys with higher strength and creep resistance, Scripta Materialia. 55 (2006) 815–818. doi:10.1016/j.scriptamat.2006.07.008.
[48] C.Y. Cui, Y.F. Gu, D.H. Ping, T. Fukuda, H. Harada, Phase Constituents and Compressive Yield Stress of Ni-Co Base Alloys, Materials Transactions. 49 (2008) 424–427. doi:10.2320/matertrans.MBW200703.
[49] C.Y. Cui, Y.F. Gu, D.H. Ping, H. Harada, Microstructural Evolution and Mechanical Properties of a Ni-Based Superalloy, TMW-4, Metallurgical and Materials Transactions A. 40 (2009) 282–291. doi:10.1007/s11661-008-9746-4.
[50] Y.F. Gu, T. Fukuda, C. Cui, H. Harada, A. Mitsuhashi, T. Yokokawa, et al., Comparison of Mechanical Properties of TMW Alloys, New Generation of Cast-and-Wrought Superalloys for Disk Applications, Metallurgical and Materials Transactions A. 40 (2009) 3047–3050. doi:10.1007/s11661-009-0032-x.
[51] C.Y. Cui, Y.F. Gu, Y. Yuan, H. Harada, Dynamic strain aging in a new Ni–Co base superalloy, Scripta Materialia. 64 (2011) 502–505. doi:10.1016/j.scriptamat.2010.11.025.
[52] R.J. Mitchell, M.C. Hardy, A nickel based superalloy, 2009.
[53] N.G. Jones, K.A. Christofidou, P.M. Mignanelli, J.P. Minshull, M.C. Hardy, H.J. Stone, Influence of elevated Co and Ti levels on polycrystalline powder processed Ni-base superalloy, Materials Science and Technology. 30 (2014) 1853–1861. doi:10.1179/1743284714y.0000000509.
[54] C.Y. Cui, Y.F. Gu, D.H. Ping, H. Harada, Phase constituents in Ni–Al–Co–Ti quaternary alloys, Intermetallics. 16 (2008) 910–916. doi:10.1016/j.intermet.2008.04.006.
[55] J.P. Minshull, S. Neumeier, M.G. Tucker, H.J. Stone, A1-$L1_2$ Structures in the Al-Co-Ni-Ti Quaternary Phase System, Amr. 278 (2011) 399–404. doi:10.4028/www.scientific.net/amr.278.399.
[56] A.A. Oni, S.R. Broderick, K. Rajan, J.M. LeBeau, Atom site preference and γ′/γ mismatch strain in NiAlCoTi superalloys, Intermetallics. 73 (2016) 72–78. doi:10.1016/j.intermet.2016.03.006.
[57] W.J. Boettinger, U.R. Kattner, K.-W. Moon, J.H. Perepezko, DTA and Heat-flux DSC measurements of alloy melting and freezing, 2006.
[58] G.S. Pawley, IUCr, Unit-cell refinement from powder diffraction scans, Journal of Applied Crystallography. 14 (1981) 357–361. doi:10.1107/S0021889881009618.
[59] D.L. Sponseller, Differential Thermal Analysis of Nickel-Base Superalloys, in: Superalloys, TMS, 1996: pp. 259–270. doi:10.7449/1996/Superalloys_1996_259_270.
[60] K. Owusu-Boahen, M. Bamberger, S.F. Dirnfeld, B. Prinz, J. Klodt, Precipitation hardening in nickel based superalloys: effect of alloying, Materials Science and Technology. 12 (1996) 290–294. doi:10.1179/026708396790165777.
[61] M. Xie, R. Helmink, S. Tin, The Influence of Cr on the Solidification Behavior of Polycrystalline γ(Ni)/γ′(Ni3Al)-δ(Ni3Nb) Eutectic Ni-Base Superalloys, Metallurgical and Materials Transactions A. 43 (2011) 1259–1267. doi:10.1007/s11661-011-0969-4.
[62] J.R. Stephens, R.L. Dreshfield, Understanding the roles of the strategic element coblat in nickel base superalloys, 2012.
[63] R.N. Jarrett, J.K. Tien, Effects of Cobalt on Structure, Microchemistry and Properties of a Wrought Nickel-Base Superalloy, Mta. 13 (1982) 1021–1032. doi:10.1007/BF02643399.
[64] J.R. Stephens, J.K. Tien, Considerations of technology transfer barriers in the modification of strategic superalloys for aircraft turbine engines, 2013.
[65] Y. Zhi'an, X. Yaotian, S. Changxu, The role of cobalt in the high temperature creep of γ′-strengthened nickel-based superalloys, Materials Science & Engineering A. 101 (1988) 65–73. doi:10.1016/0921-5093(88)90051-2.
[66] D.A. Porter, K.E. Easterling, Phase transformations in metals and alloys, Second, Taylor & Francis, n.d.
[67] S. Ochiai, Y. Oya, T. Suzuki, Alloying behaviour of Ni_3Al, Ni_3Ga, Ni_3Si and Ni_3Ge, Acta Metallurgica. 32 (1984) 289–298. doi:10.1016/0001-6160(84)90057-9.
[68] A.K. Jena, M.C. Chaturvedi, The role of alloying elements in the design of nickel-base superalloys, Journal of Materials Science. 19 (1984) 3121–3139. doi:10.1007/BF00549796.
[69] R.A. Ricks, A.J. Porter, R.C. Ecob, The growth of γ′ precipitates in nickel-base superalloys, Acta

Metallurgica. 31 (1983) 43–53. doi:10.1016/0001-6160(83)90062-7.
[70] R.W. Kozar, A. Suzuki, W.W. Milligan, J.J. Schirra, M.F. Savage, T.M. Pollock, Strengthening Mechanisms in Polycrystalline Multimodal Nickel-Base Superalloys, Metallurgical and Materials Transactions A. 40 (2009) 1588–1603. doi:10.1007/s11661-009-9858-5.
[71] R.F. Decker, Strengthening mechanisms in nickel-base superalloys, in: 2013: pp. 1–24.
[72] D. Raynor, J.M. Silcock, Strengthening Mechanisms in γ′ Precipitating Alloys, Metal Science. 4 (1970) 121–130. doi:10.1179/msc.1970.4.1.121.
[73] N.S. Stoloff, Physical and mechanical metallurgy of Ni 3 Al and its alloys, International Materials Reviews. 34 (1989) 153–184. doi:10.1179/imr.1989.34.1.153.
[74] P.M. Mignanelli, N.G. Jones, M.C. Hardy, H.J. Stone, The influence of Al_Nb ratio on the microstructure and mechanical response of quaternary Ni–Cr–Al–Nb alloys, Materials Science & Engineering A. 612 (2014) 179–186. doi:10.1016/j.msea.2014.06.021.
[75] V. Gerold, H. Haberkorn, On the Critical Resolved Shear Stress of Solid Solutions Containing Coherent Precipitates, Phys. Stat. Sol. (B). 16 (1966) 675–684. doi:10.1002/pssb.19660160234.
[76] V. Gerold, H.M. Pham, Precipitation hardening by misfitting particles and its comparison with experiments, Scripta Metallurgica. 13 (1979) 895–898. doi:10.1016/0036-9748(79)90182-0.
[77] D.A. Grose, G.S. Ansell, The influence of coherency strain on the elevated temperature tensile behavior of Ni-15Cr-AI-Ti-Mo alloys, Mta. 12 (1981) 1631–1645. doi:10.1007/BF02643569.
[78] A.J. Ardell, Precipitation hardening, Mta. 16 (1985) 2131–2165. doi:10.1007/bf02670416.
[79] B.A. Parker, On the contribution of coherence to the strength of nickel-aluminium-titanium alloys, Scripta Metallurgica. 4 (1970) 905–906. doi:10.1016/0036-9748(70)90230-9.

Table 1: Summary of actual alloy compositions measured using electron dispersive X-ray spectroscopy (EDX). The transition temperatures obtained from differential scanning calorimetry (DSC) of the as-homogenised samples are also included along with the homogenisation temperature for each sample.

Table 2: Transition temperatures calculated using Thermo-Calc and the TCNi5 and TTNi8 databases.

Table 3: Summary of lattice misfit values, hardness and γ′ size.

Figure 1: Example of the analysis of neutron diffraction data from alloy 101b using the Pawley procedure. The data is overlaid with the fitted pattern, and the residual curve is shown.

Figure 2: Secondary electron micrographs of all alloys with chromium additions of 10 at. % following homogenisation heat treatment.

Figure 3: Secondary electron micrographs of all alloys with chromium additions of 15 at. % following homogenisation heat treatment.

Figure 4: Secondary electron micrographs of all alloys with chromium additions of 20 at. % following homogenisation heat treatment.

Figure 5: Collective results showing the variation of the Vickers hardness, lattice parameters of the γ and γ′ phases and lattice misfit as a function of the concentration of Ti (in at.%) in the alloys.

Figure 6: Graphical representation of key transition temperatures obtained by DSC plotted as a function of the equivalent quantities obtained using thermodynamic modelling. a & b) Calculations performed using the TCNi5 database and c & d) calculations performed using the TTNi8 database.

Figure 7: Variation of Vickers hardness as a function of the lattice misfit. The alloys have been into three groups depending on highest concentration matrix element. The lines shown represent the best-fit lines for each group of alloys.

Table 1: Summary of actual alloy compositions measured using electron dispersive X-ray spectroscopy (EDX). The transition temperatures obtained from differential scanning calorimetry (DSC) of the as-homogenised samples are also included along with the homogenisation temperature for each sample.

Alloy	**Actual composition (at%)**					**Temperatures obtained by DSC (˚C)**			**Homogenisation Temperature (˚C)**
	Ni	**Co**	**Al**	**Ti**	**Cr**	**Liquidus**	**Solidus**	**γ′ solvus**	
101a	27.2	50.7	3.1	8.1	10.9	1376	1278	1062	1200
101b	19.7	58.5	5.4	5.3	11.0	1402	1288	963	1200
101c	19.7	59.1	7.5	2.6	11.1	>1450	1361	903	1250
102a	39.8	38.9	2.8	7.6	10.8	1378	1298	1082	1200
102b	39.2	38.1	5.9	5.3	10.5	1396	1307	1064	1250
102c	39.7	39.6	7.5	2.6	10.8	>1450	1364	999	1250
103a	58.3	19.5	3.2	8.2	10.8	1371	1302	1122	1250
103b	59.5	19.8	4.5	5.6	10.9	1392	1337	1099	1250
103c	58.4	19.6	8.6	2.7	10.7	1410	1357	1077	1250
151a	18.3	54.7	3.0	7.8	16.2	1378	1251	1055	1200
151b	18.3	53.4	5.0	5.2	16.1	1393	1295	985	1200
151c	19.0	54.7	7.1	2.7	16.5	1411	1342	916	1250
152a	37.1	35.6	3.1	7.9	16.3	1359	1264	1147	1200
152b	36.8	36.5	5.4	5.2	16.1	1385	1305	1094	1250
152c	36.1	36.6	8.6	2.7	16.0	1406	1350	1014	1250
153a	54.3	18.0	4.3	7.7	15.7	1371	1294	1135	1250
153b	54.9	18.3	5.6	5.3	15.9	1379	1301	1120	1250
153c	54.8	18.4	8.0	2.7	16.1	1399	1342	1074	1250
201a	17.3	50.3	3.1	7.9	21.5	1361	1225	1078	1150
201b	17.0	50.7	5.5	5.0	21.4	1400	1351	1080	1200
201c	17.2	50.5	7.8	2.6	21.8	1401	1311	899	1250
202a	34.2	32.6	3.6	8.1	21.5	1349	1248	1135	1200
202b	34.4	33.5	5.7	5.2	21.2	1370	1284	1071	1200
202c	34.0	33.5	8.2	2.7	21.6	1392	1302	1011	1250
203a	50.7	17.4	2.7	7.9	21.9	1341	1261	1154	1250
203b	51.2	15.7	6.0	5.5	21.6	1359	1273	1152	1250
203c	50.6	17.4	8.5	2.5	20.9	1392	1324	1088	1250

Table 2: Transition temperatures calculated using Thermo-Calc and the TCNi5 and TTNi8 databases.

Alloy	**TCNi5 prediction in ˚C**						**TTNi8 predictions in ˚C**				
	Liquidus	**Solidus**	**γ' solvus**	**η solvus**	**β solvus**	**σ solvus**	**Liquidus**	**Solidus**	**γ' solvus**	**η solvus**	**β solvus**
101a	1362	1230	962	-	-	-	1390	1331	763	1167	-
101b	1395	1290	924	-	-	-	1410	1371	923	1059	-
101c	1422	1356	773	-	933	-	1430	1410	939	-	-
102a	1370	1270	1054	1089	-	-	1390	1350	864	1236	-
102b	1400	1320	1062	-	-	-	1410	1380	1090	-	-
102c	1424	1373	1015	-	-	-	1430	1410	1054	-	-
103a	1371	1320	992	1133	-	-	1380	1351	948	1163	-
103b	1400	1360	1076	-	-	-	1410	1379	1082	-	-
103c	1420	1390	1046	-	-	-	1420	1410	1033	-	-
151a	1380	1250	882	-	-	-	1373	1310	775	1182	-
151b	1390	1260	934	-	-	-	1400	1350	945	1084	-
151c	1412	1340	747	-	999	-	1420	1390	969	-	963
152a	1360	1240	1057	1132	-	-	1380	1330	904	1255	-
152b	1390	1300	1082	-	-	-	1400	1360	1125	-	-
152c	1420	1360	1036	-	-	-	1410	1390	1054	-	-
153a	1360	1300	1008	1188	-	-	1370	1330	986	1203	-
153b	1390	1340	1108	-	-	-	1390	1370	1120	-	-
153c	1410	1371	1077	-	-	-	1410	1390	1070	-	-
201a	1340	1160	995	-	-	-	1360	1290	841	1179	-
201b	1372	1230	882	-	1020	-	1380	1330	986	-	1089
201c	1401	1313	716	-	1062	-	1400	1363	934	-	1038
202a	1350	1210	1055	1155	-	-	1353	1300	944	1256	-
202b	1380	1270	1093	-	-	756	1374	1334	1143	-	-
202c	1401	1340	1050	-	796	720	1400	1364	1074	-	-
203a	1350	1270	1019	1220	-	-	1350	1310	1021	1221	-
203b	1372	1310	1125	-	-	-	1380	1340	1140	-	-
203c	1430	1420	1093	-	-	-	1390	1370	1090	-	-

Table 3: Summary of lattice misfit values, hardness and γ′ size.

Alloy	**Lattice Misfit (%)**	**Hardness (H_v)**	**γ′ size (nm)**
101a	0.53	457	46.6 ± 0.5
151a	0.46	395	58.8 ± 0.5
201a	0.38	369	45.7 ± 0.8

Figure 1: Example of the analysis of neutron diffraction data from alloy 101b using the Pawley procedure. The data is overlaid with the fitted pattern, and the residual curve is shown.

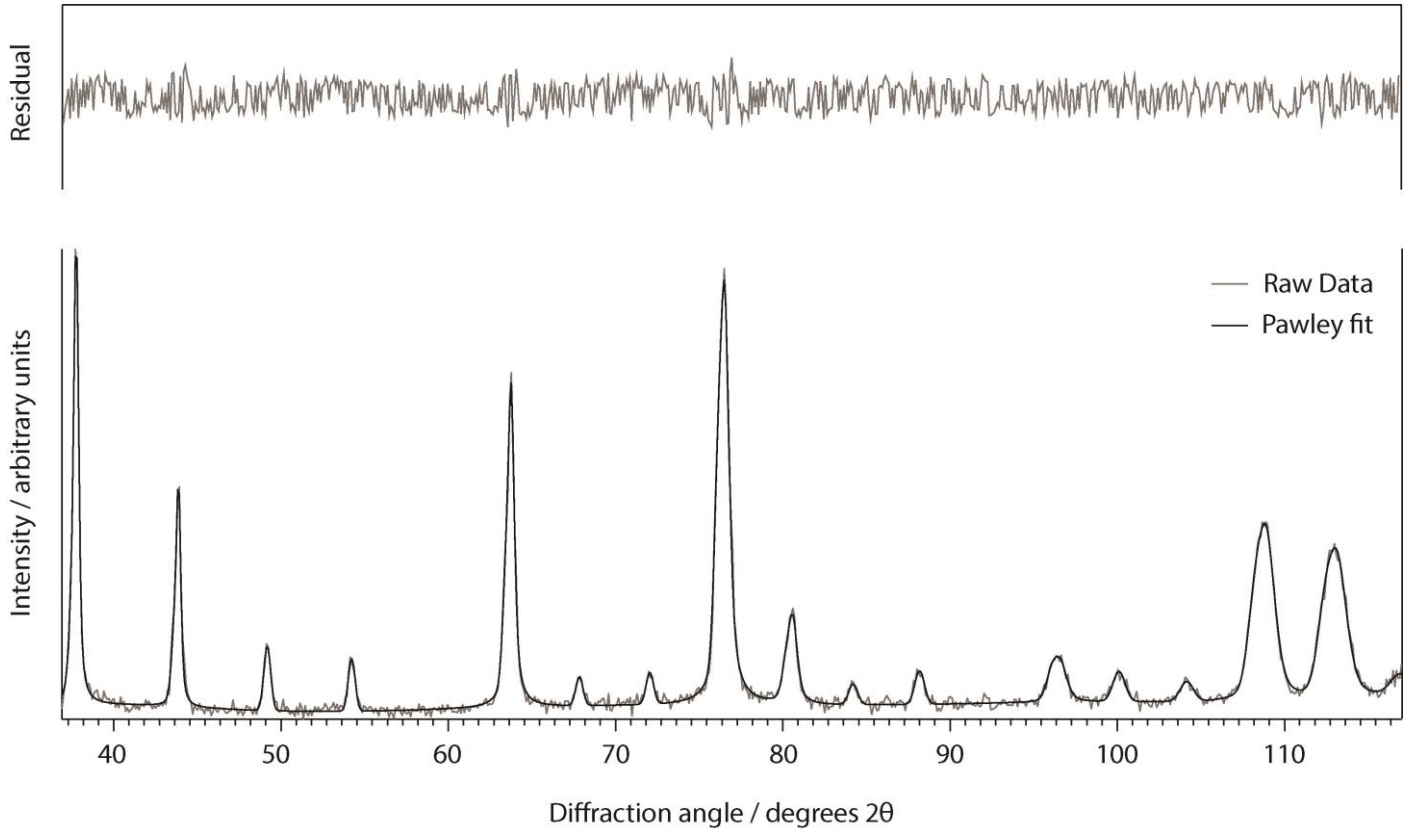

Figure 2: Secondary electron micrographs of all alloys with chromium additions of 10 at. % following homogenisation heat treatment.

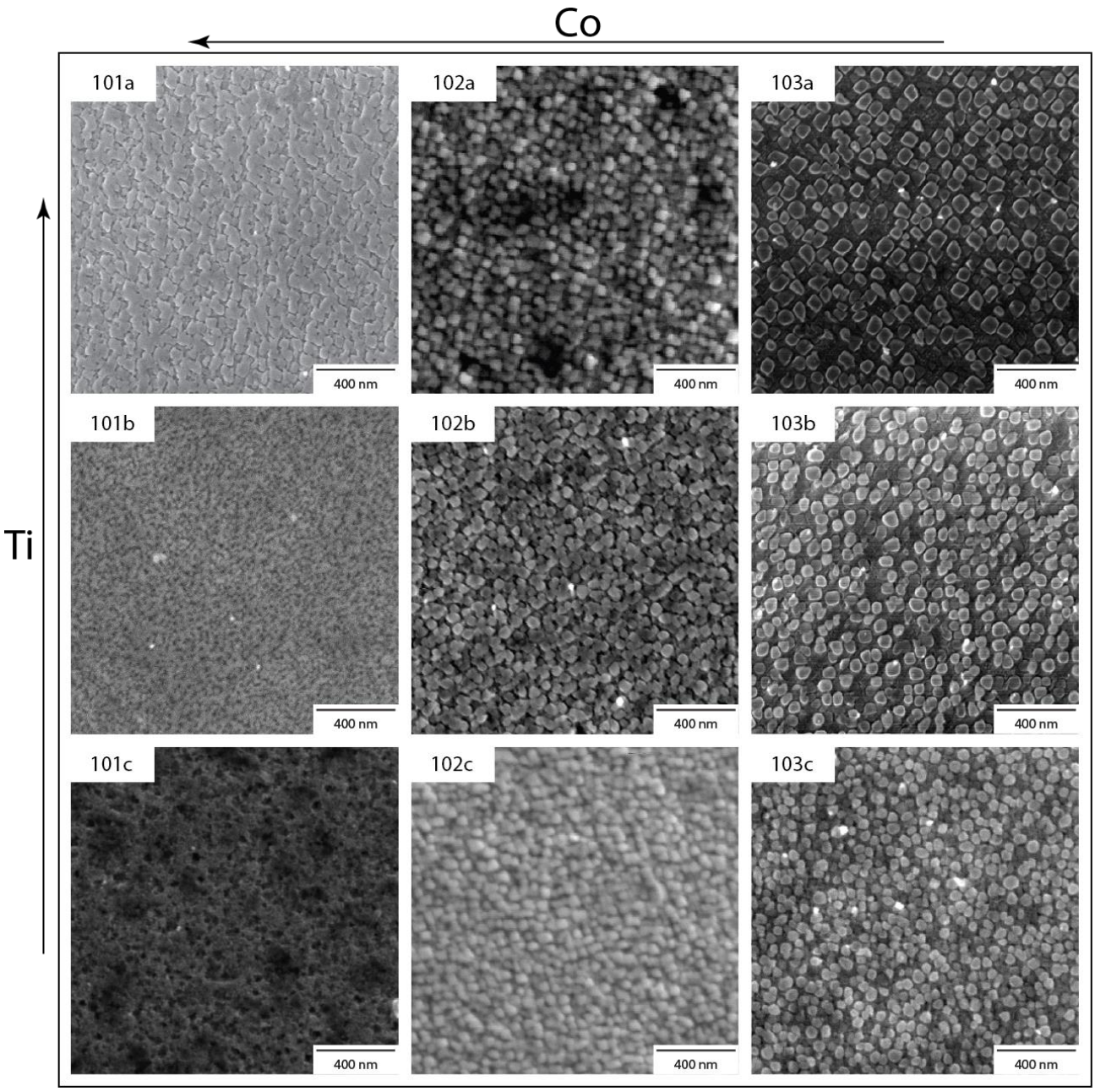

Figure 3: Secondary electron micrographs of all alloys with chromium additions of 15 at. % following homogenisation heat treatment.

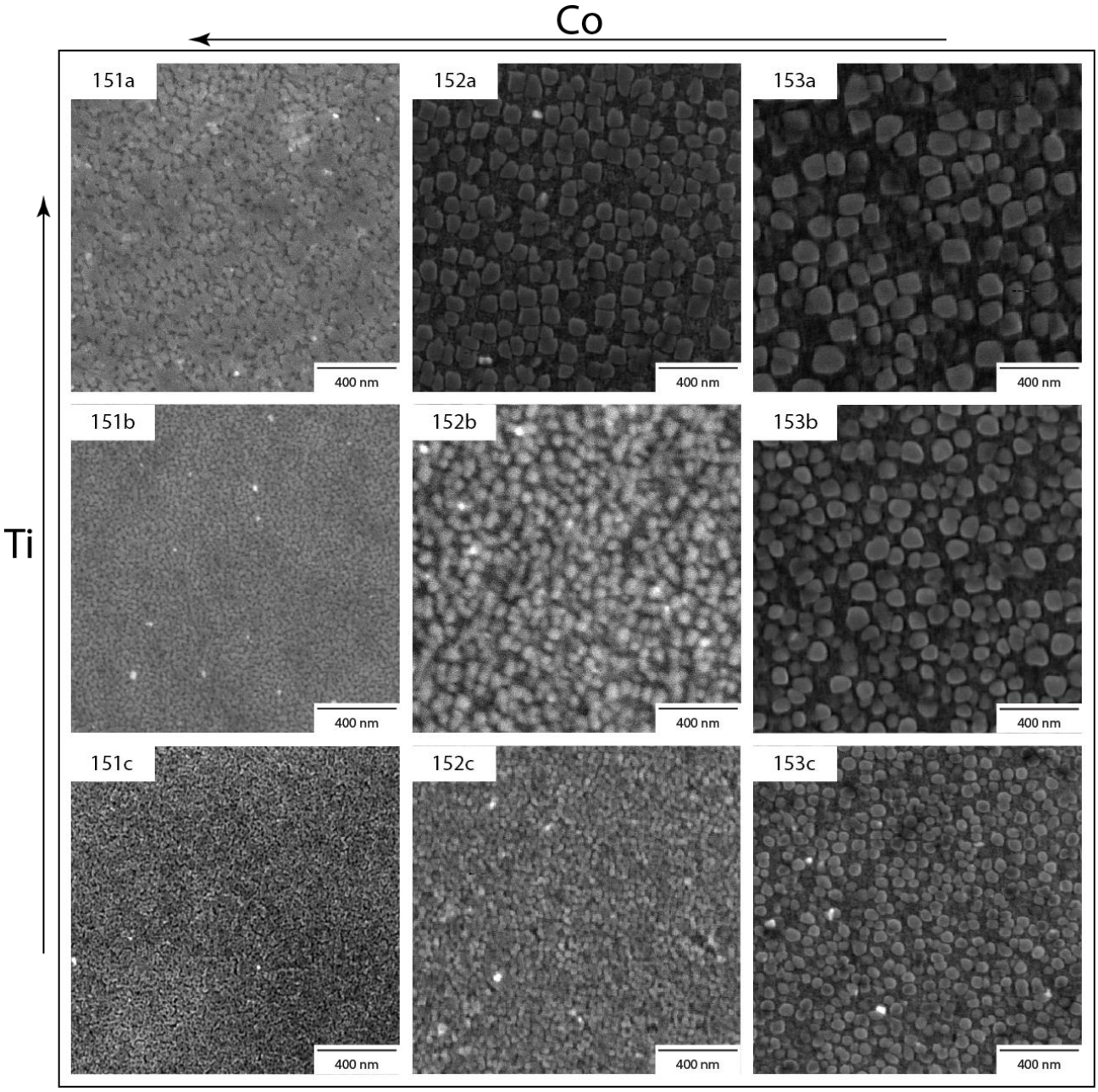

Figure 4: Secondary electron micrographs of all alloys with chromium additions of 20 at. % following homogenisation heat treatment.

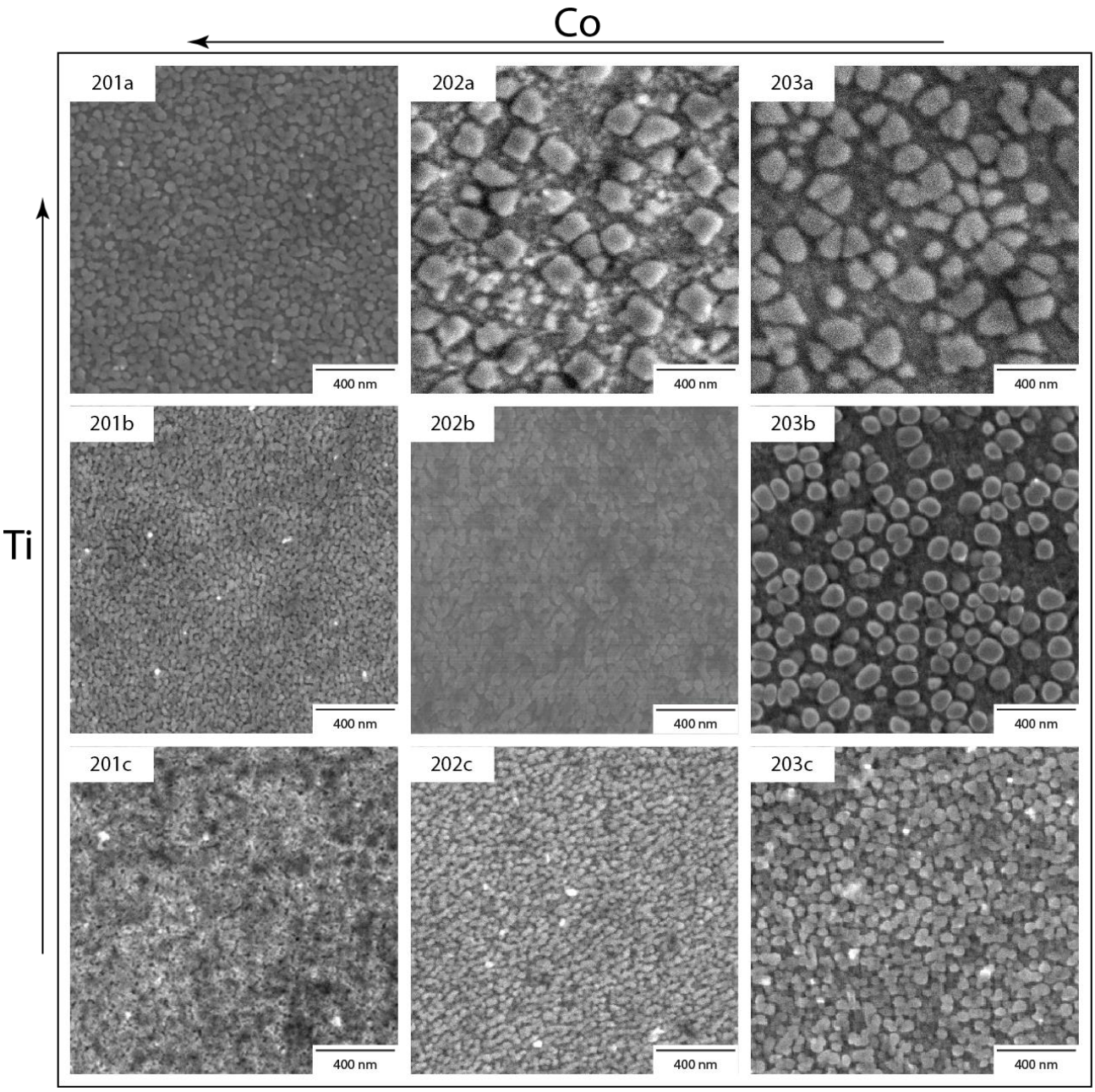

Figure 5: Collective results showing the variation of the Vickers hardness, lattice parameters of the γ and γ′ phases and lattice misfit as a function of the concentration of Ti (in at.%) in the alloys.

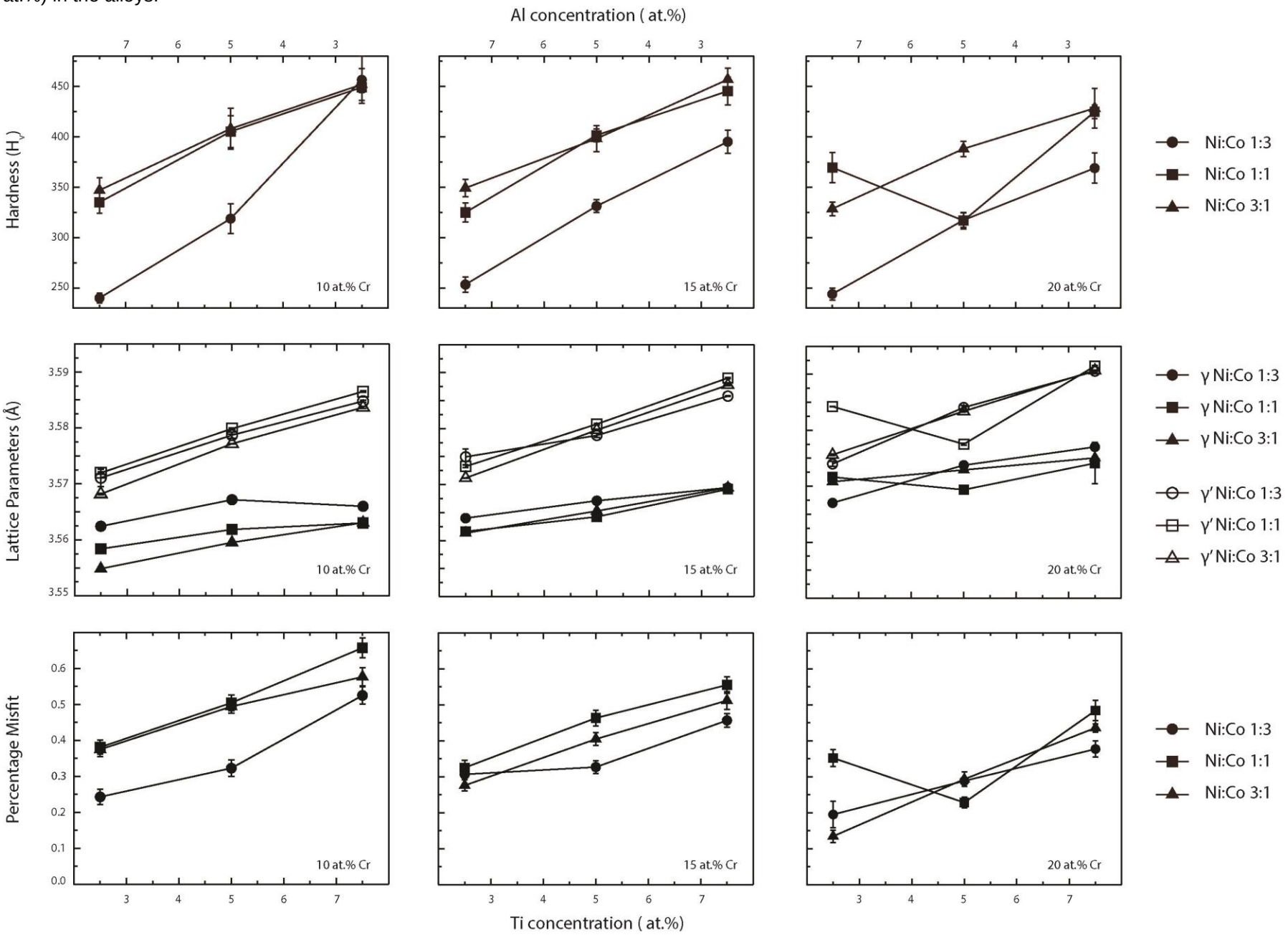

Figure 6: Graphical representation of key transition temperatures obtained by DSC plotted as a function of the equivalent quantities obtained using thermodynamic modelling. a & b) Calculations performed using the TCNi5 database and c & d) calculations performed using the TTNi8 database.

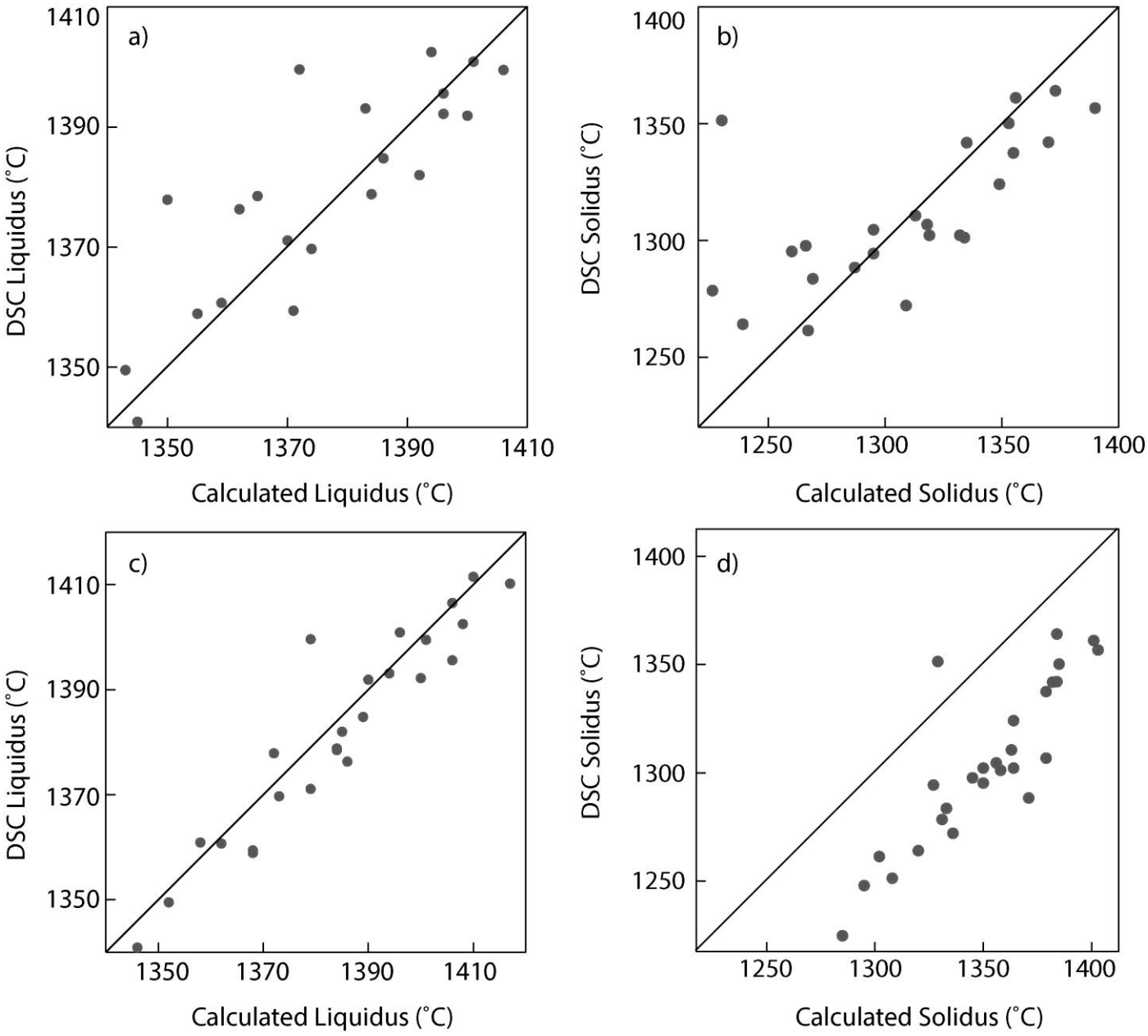

Figure 7: Variation of Vickers hardness as a function of the lattice misfit. The alloys have been into three groups depending on highest concentration matrix element. The lines shown represent the best-fit lines for each group of alloys.